AIChE

Granular Mixing and Segregation in a Horizontal Rotating Drum: A Simulation Study on the Impact of Rotational Speed and Fill Level

M. M. H. D. Arntz
Food and Bioprocess Engineering Group, Wageningen University, P.O. Box 8129, 6700 EV Wageningen, The Netherlands

W. K. den Otter and W. J. Briels
Computational Biophysics, University of Twente, P.O. Box 217, 7500 AE Enschede, The Netherlands

P. J. T. Bussmann
TNO Quality of life, P.O. Box 360, 3700 AJ Zeist, The Netherlands

H. H. Beeftink and R. M. Boom
Food and Bioprocess Engineering Group, Wageningen University, P.O. Box 8129, 6700 EV Wageningen, The Netherlands

DOI 10.1002/aic.11622
Published online November 4, 2008 in Wiley InterScience (www.interscience.wiley.com).

The rich phase behavior of granular beds of bidisperse hard spherical particles in a rotating horizontal drum is studied by Discrete Element Method (DEM) simulations. Several flow regimes and various forms of radial segregation, as well as mixing, are observed by systematically varying the operational parameters of the drum, i.e. fill level and angular velocity, over a wide range. Steady states after several dozen revolutions are summarized in two bed behavior diagrams, showing strong correlations between flow regime and segregation pattern. An entropy method quantifies the overall degree of mixing, while density and velocity plots are used to analyze the local properties of the granular bed. The percolation mechanism may provide a qualitative explanation for the distinct segregation processes, and for the transient mixing in nonradially segregated beds. Initially blockwise segregated beds are found to mix before radial segregation sets in. High fill fractions (>65%) show the most intense segregation. © 2008 American Institute of Chemical Engineers *AIChE J,* 54: 3133–3146, 2008
Keywords: radial segregation, inverted segregation, order parameter, segregation mechanism, bed behavior diagram

Introduction

Granule mixing is a common and important unit operation in the food industry. It is for example applied in freeze drying, in the production of instant soups, and to coat snacks and candies. The fundamental phenomena in granule mixing are still imperfectly understood,[1–3] making it difficult to a priori predict the effectiveness of mixing processes. Operations aimed at mixing polydisperse granules may even result in segregation. Although granular mixing has been the subject of research for some time,[2,4] the translation of the more

Correspondence concerning this article should be addressed to M. M. H. D. Arntz at marleen.arntz@wur.nl.

fundamental findings into predictions for practical processes is still sketchy. In addition, the range of parameter values studied sofar is rather limited. From this perspective, we here report a systematic study of mixing and segregation in a bed of bidisperse granules in a rotating horizontal drum, which is the simplest geometry relevant in industrial practice.

Simulations of granular materials are based on either discrete elements or continuum models. The discrete element methods (DEM) combine semi-empirical models for the interparticle interactions with the equations of motion from classical mechanics to simulate the explicit paths of all granules in the drum, thus yielding realistic predictions of the mixing process. This approach is very demanding computationally, which strongly limits the number of granules and the number of revolutions in a simulation. Continuum models dispense with the discrete particles and can therefore be scaled up more easily. But the constitutive relations that serve as the foundation for continuum modeling are difficult to come by, and often only applicable to specific systems and conditions. Here we have chosen for DEM simulations, since in this approach the phenomena emerging in the simulations are expected to be the least affected by the details and approximations of the simulation model.

In this article, DEM simulations are presented of the mixing of bidisperse, nearly incompressible, spherical granules in a rotating horizontal drum, with the aim to analyze the mixing and segregation behavior of cohesionless particles. Even in this simple system, several segregation processes are known to occur: radial segregation,[2,5–8] inverted segregation,[8,9] axial segregation,[2,10–12] radial streaking,[1,13–15] double radial segregation[9,14,16] and formation of unmixed cores.[4,17] To limit the number of possible segregation processes, we have chosen to follow Dury and Ristow[7] by focusing on quasi-2D systems, meaning that the drum has a depth of 8.3 (12.5) times the diameter of the largest (smallest) particle to suppress axial transport and thus axial segregation. The two types of particles differ in size, which at identical specific gravities implies that they also differ in mass, while the particles are identical in all other respects. Of primary interest in this study are the fill level and the rotational velocity of the drum, as it is our objective to analyze how these two easily tuneable operational parameters determine the mixing and segregation process.

Mixing and segregation in a rotating drum is believed to take place predominantly in the topmost tilted layer of the granular bed, where the particles move, individually or collectively, from one side of the drum downhill to the opposite site. Six regimes of particle flow in this flowing layer have been identified,[18,19] namely the sliding, avalanching a.k.a. slumping, rolling, cascading, cataracting and centrifuging regimes. Industrial mixing operations are typically performed in the rolling or cascading regime, and sometimes in the cataracting regime, whereas the sliding regime is avoided for its poor mixing behavior. Previous studies[1–3,6,7,20–25] have focused on a limited range of fill levels and rotational velocities, and consequently have predominantly analyzed the avalanching and rolling regimes. By considerably extending the ranges of these two operational parameters, we have been able to study the cascading, cataracting and centrifuging regimes as well. These three regimes will therefore be discussed in more detail than the rolling regime. Simulations in the latter regime are included to validate our model against previous studies, and to complete the emerging physical picture.

The simulations presented here are analyzed using a series of methods to further the understanding of the observed mixing and segregation processes, and the roles played herein by the fill factor and the angular velocity of the drum. Quantitative data on the degree of mixing, both in the steady state and as a function of time, are obtained by an entropy-based characterization method.[26–29] Density maps and velocity vector maps are used to analyze the tilted flowing layer on top of the bed. Velocity-difference vector maps are helpful in the identification of the specific regions where the small and large particles are being separated. A bed behavior diagram depicting the dependence of the flow regime on the fill level and angular velocity shows a remarkable agreement with the bed behavior diagrams collected previously for monodisperse systems.[19] The steady state degree of mixing is also plotted as a function of these two operational parameters. From this detailed analysis the general picture appears that a percolation mechanism,[30] i.e. small particles falling through the voids in the flowing layer, is responsible for translating the flow regime into a steady state segregation pattern.

This article is organized as follows: In the next section the simulation model and the aforementioned analysis methods are introduced briefly. The simulation results are presented and discussed in the results and discussion section, followed by a summary of the main conclusions in the conclusions section.

Model Description and Characterization of Mixing

Discrete element modeling (DEM)

To model time-dependent particle positions in a rotating drum, a discrete element model (DEM) is used.[29,31–34] Particles are assumed to be spherical, interacting only by contact forces both normal and tangential to their touching surfaces. The normal force exerted on sphere i by sphere j is described using a linear spring and dashpot model:

$$\mathbf{F}_{ij}^{n} = -k_n \delta_{ij} \hat{\mathbf{n}}_{ij} - \eta_n \mathbf{LC}\ \mathbf{V}_{ij}^{n}, \tag{1}$$

with k_n the elastic stiffness of the particles, δ_{ij} their apparent overlap width, $\hat{\mathbf{n}}_{ij}$ the normal unit vector from the centre of particle i to the centre of particle j, and $\mathbf{v}_{ij}^{n}$ their relative velocity along this normal. The normal damping coefficient η_n is related to the energy restitution coefficient e_{v} of particle-particle collisions.[35]

In the description of the tangential friction force one has to distinguish between the sticking and the sliding regime. In Schäfer's approximation[35] of the Coulombic friction model, the tangential force in the sticking regime reads as

$$\mathbf{F}_{ij}^{t} = -\eta_t \mathbf{v}_{ij}^{t}, \tag{2}$$

with η_{t} the viscous friction coefficient. The tangential velocity difference at the point of contact is given by

$$\mathbf{v}_{ij}^{t} = \left(\mathbf{v}_i - \mathbf{v}_j\right) - \mathbf{v}_{ij}^{n} + \left(r_i \omega_i + r_j \omega_j\right) \times \hat{\mathbf{n}}_{ij} \tag{3}$$

where $\mathbf{v}_i$, ω_i, and r_i are the velocity, angular velocity and radius of particle i, respectively. The maximum attainable fric-

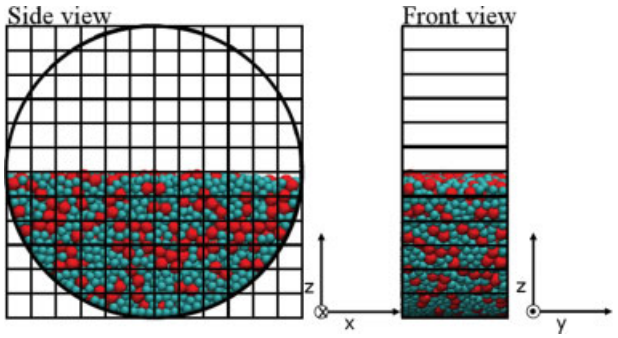

Figure 1. Front view and side view of the drum, illustrating the relative dimensions of the drum and the particles.

The straight lines show the edges of the elongated grid cells used in the calculation of the order parameter. [Color figure can be viewed in the online issue, which is available at www.interscience.wiley.com.]

tion force in the sticking regime, which is also the friction force in the sliding regime, reads as

$$\mathbf{F}_{ij}^{t} = -\mu\left|\mathbf{F}_{ij}^{n}\right|\hat{\mathbf{t}}_{ij} \tag{4}$$

with μ the Coulombic friction coefficient and $\hat{\mathbf{t}}_{ij}$ the unit vector along the tangential velocity. Note that Schäfer's approximation[35] circumvents the discontinuity in the Coulomb model by allowing the particles to slide very slowly in the sticking regime. Both normal and tangential forces cease when the particles are not in contact anymore, i.e. for $\delta_{ij} < 0$.

The interactions of particles with the drum walls are of the same form as the particle-particle interactions, where distances and velocity differences are now calculated relative to the contact point(s) with the walls. The cylindrical drum wall of radius R and length L is oriented with its rotation axis along the y-axis and is closed by flat circular walls at either end, see Figure 1. The origin of our coordinate system coincides with the center of the drum. A gravitational force pulls along the negative z-direction. The total force $\mathbf{F}_i^{\text{tot}}$ and torque $\mathbf{T}_i^{\text{tot}}$ on particle i are obtained by summation of all forces with respect to that particular particle, including contact forces exerted by the drum walls and gravity. We solve the particles' motions by numerically integrating Newton's second law of motion using the half-step 'leap-frog' scheme[36] with a fixed time step Δt.

The simulation parameters employed in this study are presented in Table 1, along with the parameters of the similar models by Dury and Ristow[7] and by Schutyser *et al.*,[37] and are discussed further in the section 'discussion of the model'. The starting configurations of our simulations were created by placing between 2000 and 8000 particles randomly in the drum, avoiding overlap, followed by a short simulation to condense the bed under the influence of gravity. By initially placing small particles on the right side ($x > 0$) and large particles on the left side ($x < 0$) of the drum, we arrived at the block-wise segregated starting configuration of Figure 2A. After all particles had settled, their velocities were set to zero before setting the drum in motion.

Analysis methods

Characterization of Mixing. Several methods to quantify the time dependent degree of mixing or segregation have been described in literature[1,2,4,6,7,38,39] Here we use a method based on the entropy of mixing[26–29] because it combines simplicity and a convenient interpretation with portability across reactor geometries and a pedigree in statistical mechanics. After defining a grid of $n_x \times n_y \times n_z$ cells, (see Figure 1), the local mixing entropy $s(\mathbf{k})$ in each grid cell $\mathbf{k} = (k_x,k_y,k_z)$ is calculated using Boltzmann's expression

$$s(\mathbf{k}) = x_a(\mathbf{k})\ln x_a(\mathbf{k}) + x_b(\mathbf{k})\ln x_b(\mathbf{k}), \tag{5}$$

where $x_x(\mathbf{k})$ is the number fraction of particles of type x in cell $\mathbf{k}$. The local entropy is defined to be zero if the cell contains no particles, or particles of one type only. The local entropies are then weighted by the number of particles in that cell, $n(\mathbf{k})$, to yield the global entropy at time t,

$$S(t) = \frac{1}{N}\sum_{k} s(\mathbf{k},t)n(\mathbf{k},t), \tag{6}$$

Table 1. Simulation Parameters in This Work and two Related Studies by Dury and Ristow[7] and Schutyser et al[30]

Description (unit)	This Work	Dury and Ristow	Schutyser et al.
Radius particle a, r_a (mm)	1.0	1.0	4.9
Radius particle b, r_b (mm)	1.5	1.5	–
Total volume fraction a/b	1	1	Monodisperse
Number of particles	2000–8000	≃300–17,000	36,000
Number ratio N_a/N_b	3.375/1	3.375/1	Monodisperse
Drum length L (mm)	25	25	220
Drum radius R (mm)	35	35	350
Specific gravity ρ (kg m^{-3})	2500	2500	2900
Restitution coefficient particle-particle e_v (–)	0.831	0.831	0.1
Restitution coefficient particle-wall e_v (–)	0.9	0.9	0.1
Dynamic interparticle friction coefficient μ (–)	0.5	0.19	0.5
Dynamic particle-wall friction coefficient μ (–)	1.5	0.6	1.5
Viscous interparticle friction coefficient η_t (kg s^{-1})	1.0	–	1.0
Viscous particle-wall friction coefficient η_t (kg s^{-1})	3.0	–	3.0
Stiffness coefficient k_n (Nm^{-1})	125	60,000	125
Time step Δt (s)	2×10^{-6}	Unspecified	2×10^{-5}
Fill level (%)	25–92	10–95	25
Rotational speed drum ω (rad s^{-1})	1.57–28	1.57	0.05–0.21

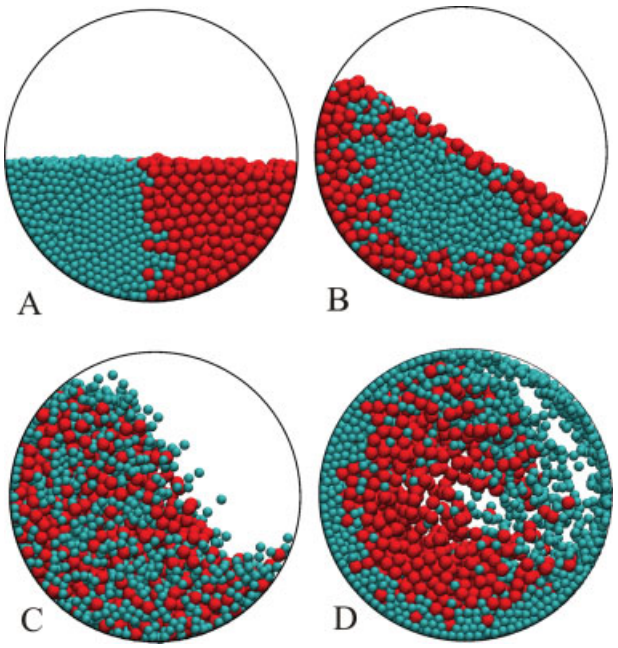

Figure 2. Four snapshots depicting cross-sections of half-filled drums at various angular velocities of the drum, with the large (small) particles drawn in dark (light) gray.

The four pictures correspond to the four marked points in Figure 3, showing (A) the blockwise segregated starting configuration, (B) a radially segregated drum in the rolling regime, (C) a well mixed bed in the cascading regime and (D) an inverse segregated drum in the cataracting regime. [Color figure can be viewed in the online issue, which is available at www.interscience.wiley.com.]

where $N = \sum_k n(\mathbf{k})$ is the conserved total number of particles. The global entropy is finally normalized, relative to the average global entropies S_{mix} of perfectly mixed and S_{seg} of perfectly segregated systems. The global entropies of these reference states are calculated by running the above procedure on sets of randomly created homogeneously mixed and fully segregated systems. This normalization procedure leads to a conveniently scaled mixing parameter,

$$\phi(t) = (S(t) - S_{\text{seg}})/(S_{\text{mix}} - S_{\text{seg}}), \tag{7}$$

with $\phi = 1$ for a mixed system and $\phi = 0$ for a fully segregated system. In contrast to several earlier methods,[6,40] the current method is readily applied to different types of segregation. For small cubic grid cells, $\{n_x, n_y, n_z\} > 1$, the method detects any kind of segregation; using bar-like cells aligned along the cylinder axis, $\{n_x, n_z\} > 1$ and $n_y = 1$, makes the method specific for radial segregation; slices perpendicular to the cylinder axis, $n_x = n_z, = 1$ and $n_y > 1$, render the technique sensitive to axial segregation. Here we follow the second approach, with $n_x = n_z$, to arrive at the grid depicted in Figure 1. We emphasize that this mixing parameter is not meant as an exhaustive characterization of the ordering in the system. For example, a radially segregated state with a core of small particles will have approximately the same mixing parameter as the inverted segregated state with a core of large particles (see Figures 2 and 3). After visual inspection of snapshots and movies made from the simulations with the VMD package,[41] we defined a system as 'mixed' at $\phi > 0.9$ and as 'segregated' at $\phi < 0.65$, with intermediate values indicating a partially segregated state.

To evaluate the influence of the grid dimensions n_x and n_z on the mixing parameter, we calculated ϕ for one simulation using a variety of grid sizes. As Table 2 shows, grids containing 10×10 to 28×28 cells yield nearly identical mixing parameters of 0.57 ± 0.03 in the steady state. Grids of less than 10×10 cells yield a spurious rise of the mixing parameter, indicating that they are too coarse to capture the segregated structure. For grids with more than 28×28 cells, the cells do not contain sufficient particles to be representative and the entropy of the well-mixed state S_{mix} deviates too much from the theoretical value of -0.54. Moreover, the widths of these cells are smaller than the diameter of the bigger particle. In this article we have chosen for a grid of 12×12 cells.

To establish the reproducibility of our simulation results and to estimate the confidence interval of the mixing parameter, a dozen microscopically distinct, yet macroscopically identical block-wise segregated configurations were created by changing the seed of the random number generator. The simulations started from these configurations display very similar dynamics, with inter-simulation fluctuations in $\phi(t)$ characterised by a standard deviation of about 0.03 at any time t after the start of the simulation. It appears, therefore, that the evolution on the macroscopic level is rather insensitive to the microscopic details, and hence the process is sufficiently repeatable to be of practical relevance. We will consider configurations to be equivalently mixed if their mixing parameters differ by less than 0.03.

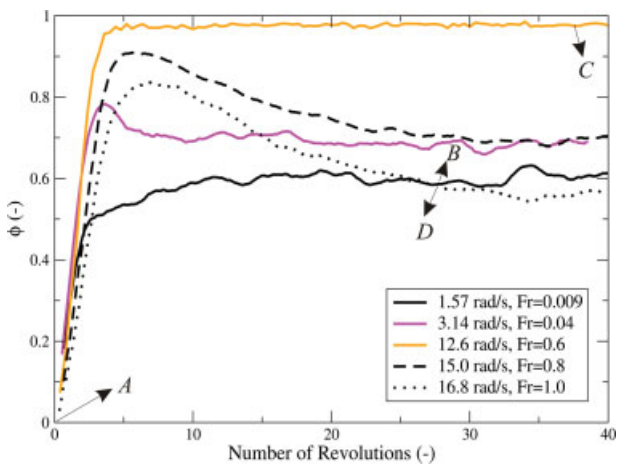

Figure 3. The degree of mixing, as calculated by the entropy method discussed in the Characterization of Mixing section, plotted against the number of drum revolutions at five angular velocities.

The simulations start with a blockwise segregated drum, at 50% fill level. Snapshots of the bed at the four marked points are presented in Figure 2. [Color figure can be viewed in the online issue, which is available at www.interscience.wiley.com.]

Table 2. Influence of the Number of Grid Cells on the Mixing Parameter ϕ in the Steady State of a Simulation with Fill Level 50%, ω = 1.57 rad/s and Other Parameters as in Table 1

No. of Cells $n_x \times n_z$	Cell Size[a]	No. of Particles Per Cell[b]	ϕ[c]	S_{seg}	S_{mix}
16	5.8	491	0.77	−0.09	−0.54
36	3.9	233	0.67	−0.08	−0.54
64	2.9	143	0.64	−0.07	−0.53
100	2.3	98	0.60	−0.06	−0.53
144	1.9	70	0.58	−0.06	−0.53
196	1.7	51	0.58	−0.06	−0.53
256	1.5	41	0.57	−0.05	−0.52
324	1.3	32	0.56	−0.05	−0.52
400	1.1	26	0.56	−0.05	−0.52
484	0.9	22	0.56	−0.05	−0.51
576	0.9	19	0.55	−0.05	−0.51
784	0.8	14	0.54	−0.04	−0.50
1296	0.6	9	0.52	−0.04	−0.46

The entropies S_{seg} and S_{mix} are obtained by averaging over sets of randomly produced segregated and mixed configurations, respectively, under identical conditions.
[a]In multiples of the largest particle diameter.
[b]Average number of small and large particles in occupied cells.
[c]Order parameter after 35 revolutions.

Bed Expansion. Bed density plots, like Figure 4A and 4D, give impressions of the global and local expansions of the bed and the distribution of voids during mixing and segregation. The drum is divided into 28 × 28 cells along the *xz* plane and the occupied volume per cell is averaged over the last 10 revolutions of the simulations. These values are then normalized by the accessible volumes of the cells, to account for the restrictions posed by the hard walls. Density plots in which only one type of particle is taken into account (not shown) clearly illustrate the radial cores of small particles for low rotational speeds and of large particles for high angular velocities of the drum. Because of the quasi 2D geometry of the drum, we do not observe any appreciable axial segregation in analogous density plots along the *xy* and *yz* planes (not shown).

Local Velocities. Velocity vector plots are made with the same grid cells as the bed expansion plots, using a mass-weighted average of the particle velocities in the *x* and *z*

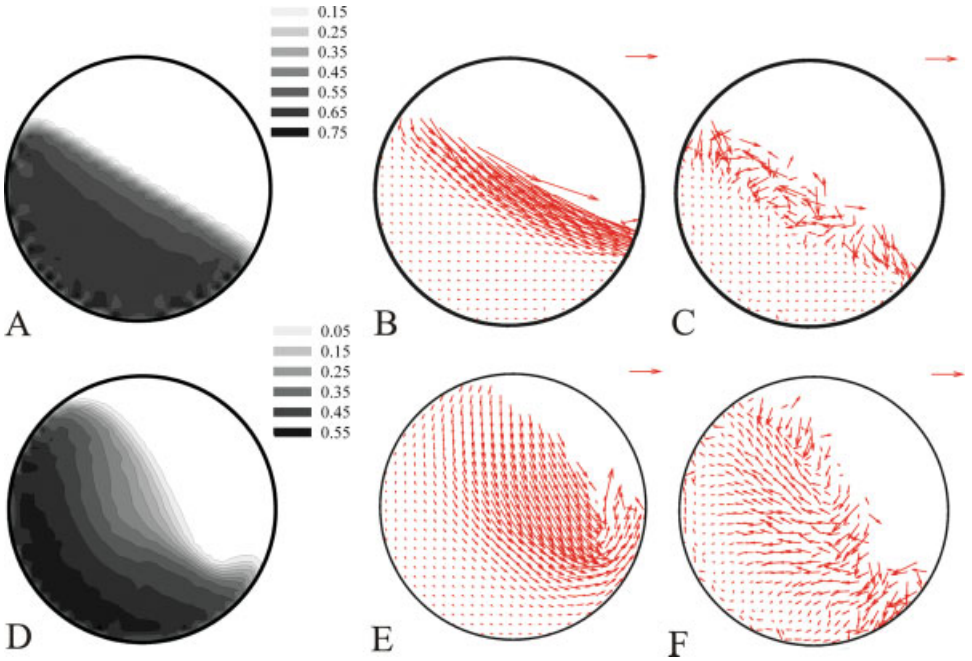

Figure 4. Analysis of the bed properties in a rotating drum at 50% fill level, for angular velocities in the rolling regime (1.57 rad/s; plots A, B, and C) and the cascading regime (12.56 rad/s; plots D, E, and F).

From left to right: the local density of the bed (plots A and D), the average velocity of the particles relative to a rigid body rotation ($\mathbf{v}_i - \boldsymbol{\omega}_d \times \mathbf{r}_i$; plots B and E, with the reference vectors in the top right corner representing 0.1 and 0.8 m/s respectively), and the segregational velocity difference between small and large particles ($\mathbf{v}_a - \mathbf{v}_b$; plots C and F with the reference vectors in the top right corner indicating 0.01 and 0.03 m/s, respectively). [Color figure can be viewed in the online issue, which is available at www.interscience.wiley.com.]

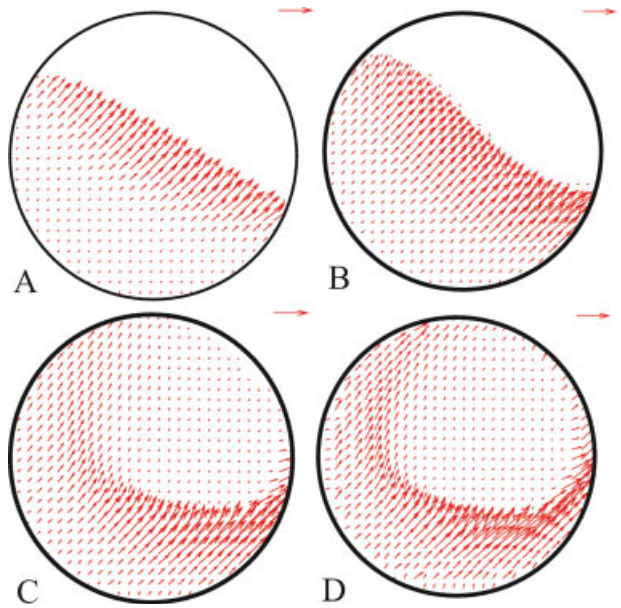

Figure 5. Vector plots of the standard deviations in the particle velocities, for 50% filled drums in a steady state at (A) 1.57 rad/s, (B) 6.28 rad/s, (C) 16 rad/s, and (D) 18 rad/s.

The x and z components of the vectors represent the standard deviations in the local particle velocities along the x and z directions, respectively. The reference vectors in the four plots correspond to 1/80, 1/60, 1/35, and 1/50 m/s respectively. [Color figure can be viewed in the online issue, which is available at www.interscience.wiley.com.]

directions. These plots, e.g. Figures 4B, E, clearly illustrate where the motion of the granular bed deviates from a solid body rotation around the axis of the drum. The net segregation/mixing flux is nicely visualized as the difference between the local average velocities of large and small particles, see Figures 4C, F. These velocity difference plots are made for homogeneously mixed systems, in which the averaging covers only a short timespan before significant demixing sets in. For clarity, grid cells containing merely one type of particles are omitted in the difference plots. To study the effect of dispersion by random collisions (also called random collision diffusivity), we have also calculated the standard deviations of the x and z velocity components of the particles, per particle type and per cell, as shown in Figure 5.

Discussion of the Model. The employed simulation model is largely based on the model by Dury and Ristow,[7] but differs from their model in several respects. To create a simple model with few tunable parameters, our implimentation does not include the tangential deformation forces introduced by Walton and Braun[42] and Cundall and Strack,[31] nor do we have a rolling friction with the wall[7]: these forces are only relevant at low or vanishing rotational drum velocities,[35] while we are interested in the higher angular drum velocities required for the rolling regime and beyond. The model parameters listed in Table 1 are derived from the parameters employed by Dury and Ristow,[7] and supplemented with elasticity and friction coefficients from Schutyser et al.[29] These coeffients lie in the typical ranges employed in various simulation studies.[43,44] In a fortcomming article we present a discussion of these parameters, showing that the bed dynamics is relatively insensitive to the precise values of these coefficients, with significant deviations in the bed dynamics occurring only for values well outside the conventional ranges. Since the time step of the integration algorithm is mainly determined by the elastic stiffness k_n of the particles, we have opted for a relatively low elasticity $k_n = 125$ N/m to make longer simulations feasible. Here again, the precise value is of limited practical effect as long as the particles possess a well-defined excluded volume. The maximum allowed time step follows from the condition that the equations of motion should be integrated sufficiently accurately. Schäfer's criterion[35] suggests $\Delta t = 0.01\tau$, with τ the collision time, but our tests on conservation of linear and angular momentum (and on conservation of energy for $e_v = 1$) for binary collisions and on conservation of energy in partially filled drums suggested a smaller time step of 0.0025 τ is needed to ensure accuracy. Visual inspection of a half-filled drum rotating at a quarter revolution per second showed that our model behaves similar to that of Dury and Ristow[7] (not shown), in further support of the above expressed viewpoint that the differences between the models are of little relevance at the simulated angular drum velocities.

To assess the influence of the end walls of the drum in the current quasi-2D geometry, with a drum length amounting to 8.3 (12.5) times the diameter of the largest (smallest) particle, the simulations of the aforementioned half-filled reference system of Dury and Ristow[7] were repeated for two different drums. Neither a drum with periodic boundary conditions along the axial direction nor a drum with a doubled drum length revealed any significant differences from the standard geometry. An obvious effect of the limited drum depth is the suppression of axial segregation, as desired in this study on radial segregation.

A number of general observations, which the bidisperse system shares with the monodisperse systems of Nakagawa[45] in the rolling regime, are illustrated in Figure 4. We see that the bed can roughly be divided in two parts, see Figure 4B: the passive bulk in which particles undergo solid body rotation around the cylinder axis and the active layer in which the particles undergo collective linear translation due to the sliding motion. In the latter layer the particles also experience a diffusional/random motion relative to each other, resulting from interparticle collisions (Figure 5A). The bed density increases moving along the surface normal from the free surface of the bed down to the passive bulk, see Figure 4A. The velocity parallel to the free surface varies along the flowing layer with a maximum approximately halfway down the slope, see Figure 4B, where the layer thickness and the diffusional motion also reach a maximum, see Figures 4A and 5A. Similar results have been obtained in experiments on bidisperse and monodisperse systems,[45] strengthening our confidence in the model.

In previous studies, it has been assumed that the flow regimes are unequivocally characterized by the Froude number, defined as the dimensionless ratio of centrifugal and gravitational forces,[2,9]

$$Fr = \omega_d^2(R - r_x)/g, \tag{8}$$

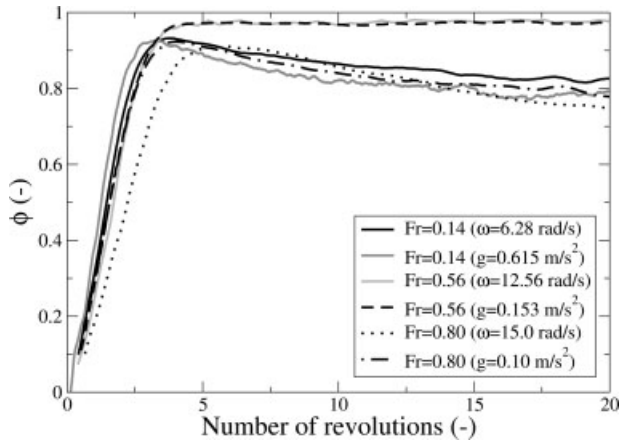

Figure 6. The order parameter as a function of time, illustrating the effect of the Froude number on the mixing dynamics of the half-filled drum.

The Froude number was varied either by changing the angular velocity of the drum (at $g = 9.81$ m/s^2) or by changing the gravitational acceleration (at $\omega_d = 1.57$ rad/s). The simulations lasted for a total of 40 revolutions, but all significant changes in the order parameters occurred inside the depicted range of revolutions.

with ω_d the angular velocity of the drum and g the gravity acceleration. To validate this assumption, three simulations were performed at $Fr = 0.14$, 0.56 and 0.8 by varying the rotational speed of the drum at fixed standard acceleration of $g = 9.81$ m/s^2. Three additional simulations were performed at identical Fr values by varying the gravitational acceleration at a constant rotational speed of a quarter revolution per second. In Figure 6 we see small differences between each pair of mixing parameter curves at identical Fr, especially in the first 5 revolutions at the largest Fr value. Apparently, the process dynamics at high Fr values are not completely characterized by this dimensionless number, but since this effect is small it is disregarded and Fr will be used in this study as the parameter determining the flow regime.

Results and Discussion

In this section the results of our simulations are presented and discussed. The two operational parameters of the system, namely the angular velocity and the fill level, have been varied systematically to study their impact on (the evolution of) the mixing/segregation process; all other system parameters are kept fixed as stated in Table 1. The first subsection describes the effect of the drum velocity for a half filled drum, the next subsection analyses the influence of the fill level at constant angular velocity, and in the third subsection both parameters are varied systematically to scan the parameter space.

Rotational velocity

The angular velocity of the drum is an important operational parameter. We first study its influence on the segregation and flow regimes in the steady state, followed by a discussion of how the various flow regimes may explain the evolutions of the distinct segregated states.

Steady State. The steady state mixing parameter ϕ of a half-filled drum in the steady state, i.e. after 30 revolutions, is depicted in Figure 7 as a function of the Froude number. The degree of mixing first increases with the rotational speed, exhibits a broad maximum, and then rapidly decreases again. Visual inspection of the simulations reveals that these three regimes roughly coincide with three different ordering regimes and with three different flow regimes; the latter are identified using the criteria of Mellman.[19] At relatively low rotational speeds radial segregation takes place ($10^{-4} < Fr < 0.023$; region RS in Figure 7), while the flow profile is characteristic of the rolling regime ($10^{-4} < Fr < 0.035$; region RO in Figure 7). At intermediate speeds the system mixes relatively well ($0.25 < Fr < 0.68$; region MX in Figure 7). The flow profiles observed in this regime are indicative of cascading ($0.12 < Fr < 0.46$; region CS in Figure 7), with a gradual transition to cataracting ($0.46 < Fr < 0.68$). At high rotational speeds inverted segregation sets in ($0.85 < Fr < 1.4$; region IS in Figure 7), coinciding with the cataracting profile ($0.77 < Fr < 1.0$; region CT in Figure 7) and the transition flow profile between cataracting and centrifuging flow ($1.0 < Fr < 2.23$). Please note that this latter system may not completely have reached steady state yet due to its slow re-ordering dynamics. With increasing angular velocity the centrifuging regime ($Fr > 2.23$; not shown in Figure 7) is established. In this regime the whole system is stagnant with the centrifuging particles forming a layer covering the entire wall. The observed relation between the flowing

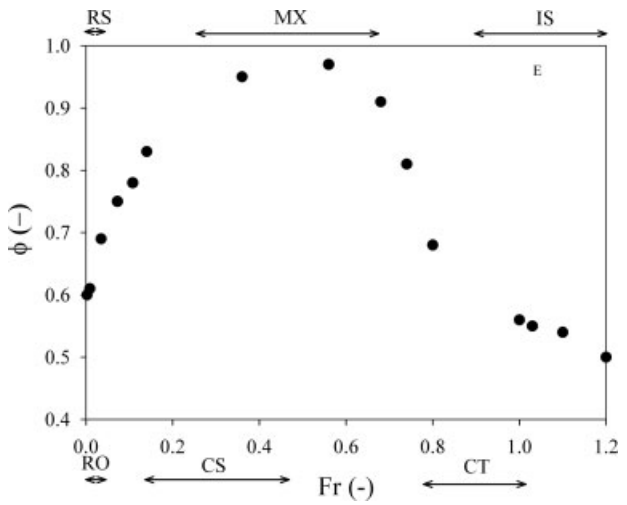

Figure 7. The mixing parameter ϕ of the steady state in half-filled drums with various rotational velocities, plotted against the corresponding dimensionless Froude number.

The ranges of different flow regimes are marked at the bottom, with "RO" denoting rolling, "CS" for cascading and "CT" for cataracting. At even higher Froude numbers, $1.0 < Fr < 2.23$, the cataracting-centrifuging regime is observed, finally progressing into a centrifuging regime for $Fr > 2.23$. The ordering regimes are highlighted at the top, with "RS" for radial segregation, "MX" for mixing and "IS" for inverted segregation.

regime and the segregation/mixing process will be investigated further in the next section.

Segregation Processes. In this paragraph we focus on the formation process of the steady states for the different flow regimes.

Rolling. In the rolling regime, segregation is believed to proceed by selective percolation of the smaller particles through the flowing layer.[30] Because of the motion of the particles rolling down the inclined surface (Figure 4B), the top layer has expanded (Figure 4A), resulting in a relatively high porosity in comparison to the bulk of the bed. By virtue of their size, small particles have a higher chance of falling downwards through a pore than the large particles. This leads to a difference in average velocities between the small and large particles in the flowing layer as illustrated in Figure 4c. This segregation is visible throughout the flowing layer by the downward pointing arrows, except for a thinly populated toplayer without systematic segregation. From Figure 4b it can be seen that the passive bulk of the bed mainly rotates uniformly with the drum, and therefore no segregation or mixing takes place in this part of the bed (see also Figure 5A).

Cascading. Increasing the rotational speed of the drum to the cascading regime leads to an increase in the thickness of the flowing layer (Figure 4D). This expansion, especially in the topleft part of the flowing layer, implies the presence of many large voids, which makes the percolation mechanism less selective on the particle size, see Figure 4F, and causes mixing of the particles. The transient part of the mixing curve is independent of the drum velocity within the cascading regime, from 5 to 12 rad/s, whereas the plateau value gradually increases with the rotational velocity of the drum.

At this point, it is interesting to temporarily eliminate the steric effects from the simulations. We therefore, briefly focus on a monodisperse system with particles of the smaller type. The particles are assigned a color depending on their initial positions in the drum, thus creating a block-wise start configuration. We observe that with increasing rotational speeds of the drum, up to 5 rad/s, fewer drum rotations are needed to obtain a mixed state, see Figure 8. In the cascading regime, ranging from 5 to 12.56 rad/s, however, the mixing profile ϕ is independent of the angular velocity. This constant profile coalesces with the mixing curve of the bidisperse system at $\omega = 12.56$ rad/s, suggesting that the mixing process has become insensitive to the particle sizes at this particular velocity and fill level. At even higher angular velocities the system requires increasingly more revolutions to reach its steady state. We now discontinue the discussion of the monodisperse system, and return to the regular system with bidisperse particles.

Cataracting. In the cataracting regime the flowing layer is characterized by particles from the bed being flung into the previously void space above the bed,[19] as shown in Figures 9A through C. The flowing layer can now be subdivided into three distinct regions. From left to right, we first pass a region where particles are thrown into free space by the high velocities acquired in the bed. The particles nearest the drum wall have the highest velocities, reach the highest altitude and are thrown the furthest. Next comes a region where the velocities are too low to throw the particles, and instead the particles roll down the steeply inclined flowing layer, see Figures 9A, B. This rolling motion is also evident from

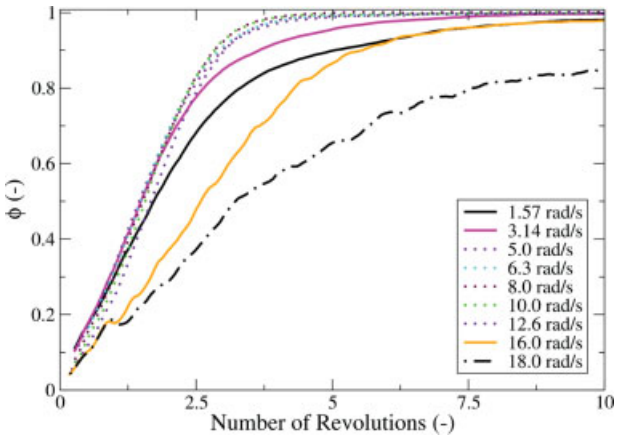

Figure 8. The mixing behavior of a 50% filled monodisperse system containing equal amounts of red and blue particles in a block-wise segregated starting configuration, for various angular velocities of the drum.

Note that the curves for $\omega_d = 5$ to 12.6 rad/s are identical to within about 0.03. The simulations lasted for at least 40 revolutions, with the most significant changes in de order-parameters occuring inside the depicted range of revolutions. Only the order parameter at the highest drum velocity continues to rise after the tenth revolution, reaching $\phi = 0.87$ after 50 revolutions.

Figure 10A, where the distribution of the average angular velocity component $\omega_{i,y}$ parallel to the drum axis is depicted. In the third region of the flowing layer, at the bottom right of the drum, the rolling and flying particles meet again to settle into a densely packed bed for the next revolution. After a number of revolutions a steady state of inverted segregation is reached, with the small particles concentrated on the outside and the large particles on the inside of the drum.

It has been argued[9,46] that the key to inverted segregation lies in two mass-related phenomena: gravity causing particles to fall down and inertia giving rise to centrifugal effects. The former dominates at the low angular drum velocities in the rolling and cascading regimes, where regular radial segregation or mixing is observed, while the latter takes precedence at the higher drum velocities in and beyond the cataracting-centrifuging regime, which display inverted segregation. A balance between the two is reached at $Fr = 1$ (see Eq. 8), corresponding with the critical angular velocity ω_c at which the outermost layer of particles starts to centrifuge. The particle radius dependence of ω_c instigated Ninayand[8] and Turner and Nakagawa[9] to suggest that inverted segregation arises because the centrifugal effects are slightly stronger for the smaller particles than for the larger particles. In the current system these critical angular velocities are $\omega_{c,a} = 16.99$ rad/s and $\omega_{c,b} = 17.11$ rad/s, suggesting that the difference is probably too small to explain inverted segregation. We furthermore note that inverted segregation is already observed at 15.5 rad/s ($Fr = 0.85$), well below the critical angular drum velocity of either particle.

For new insights into the physics of the segregation process we return to the distributions depicted in Figure 9. The velocity difference plot of Figure 9C shows a pronounced region of separation activities near the bottom and bottom

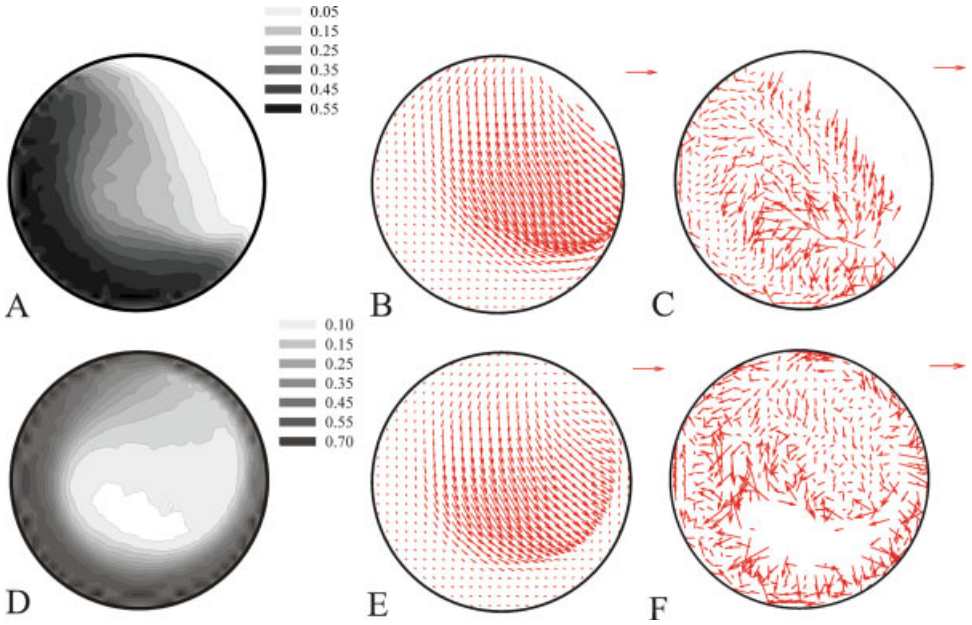

Figure 9. Analysis of the bed properties in rotating half full drums in the cataracting regime (15 rad/s ; plots A, B and C) and the cataracting-centrifuging regime (19 rad/s; plots D, E and F), showing the density (A and D), relative velocity (with the reference arrows in the top right corner representing 0.73 and 0.76 m/s, respectively) and velocity difference (C and F with the reference arrows in the top right corner indicating 0.024 and 0.019 m/s, respectively).

See the caption of Figure 4 for more details. [Color figure can be viewed in the online issue, which is available at www.interscience.wiley.com.]

right of the drum, where the smaller particles are moving down relative to the large particles. This region roughly coincides with the settling region in the above discussion of the flowing layer, and with a low density region in Figure 9A. It appears therefore that inverted segregation is caused by small particles percolating through the voids in an expanded bed, i.e. the same mechanism also underlying regular radial segregation. The main difference between the two segregation processes is the location of the percolation region. In the rolling regime the percolation takes place along the entire length of the flowing layer, i.e. the full width of the drum, with the smaller particles sinking down until they reach the denser central core of small particles. In the cataracting regime the percolation occurs mainly at the right side of the drum, where the small particles sinking down quickly reach the drum wall. We believe, therefore, that a single mechanism explains both regular and inverted segregation.

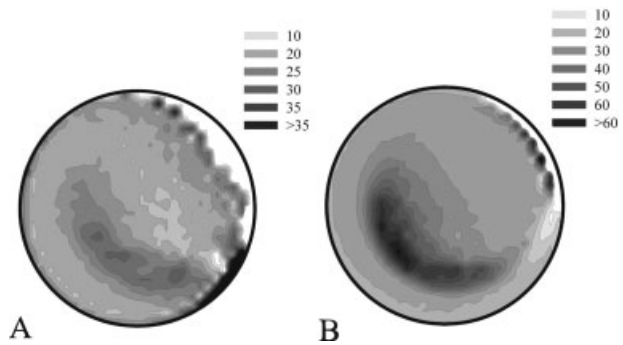

Figure 10. Distribution of the axial (*y*) component of the angular velocities of the particles for drum angular velocities of 15 rad/s (left) and 19 rad/s (right).

Note that the particles in the regions of low density, <0.05 volume fraction near the top right for 15 rad/s and just below the center at 19 rad/s, are spinning with the highest angular velocities.

Cataracting-centrifuging. The cateracting-centrifuging regime has similar characteristics to the cateracting regime, see Figures 9D through F and 10B, with the main difference that some particles stack into one or more closely packed centrifuging layers covering the entire wall, while the remaining particles still form a bed in the cataracting regime. Combining Figures 9D, F, one sees that percolation of the smaller particles is now predominantly taking place at the right and bottom side of the drum, but the relatively high particle density in this region makes it a tedious process, and hence inverted segregation is established only very gradually. This again suggests that the main mechanism of inverted segregation is percolation, rather than the difference in critical rotational speed. At increasing angular drum velocities the fraction of particles in centrifuging layers increases, these layers become denser and more immobilized, making percolation an increasingly unlikely process. The reduced transport in this regime is also seen in the monodisperse system (Figure 8) and in the standard deviation plots of Figure 5. Higher angular drum velocities effectively immobilize the particles, trapping the system in a state of incomplete inverted segregation.

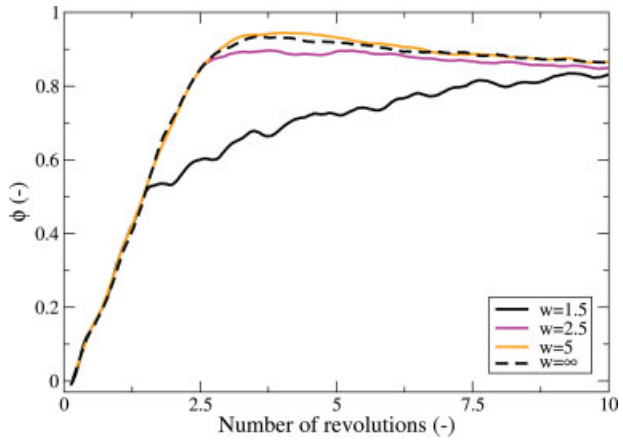

Figure 11. Reversing the rotational direction of the drum every *w* revolutions, in half-filled drums rotating at ±6.28 rad/s, affects the evolution of the order parameter while the steady state remains essentially unaltered.

The simulations lasted for a total of 40 revolutions, but all significant changes in the order parameters occurred inside the depicted range of revolutions. [Color figure can be viewed in the online issue, which is available at www.interscience.wiley.com.]

Initial mixing. The percolation mechanism may also explain the transient dynamics of the mixing parameter, whose typical development can be seen in Figure 3. Starting from a block-wise segregated configuration with $\phi = 0$, the mixing parameter passes through a maximum before reaching a steady state. From visualizing numerous simulations, the general picture emerges that the block-wise segregated bed is always being mixed thoroughly in the first couple of revolutions of the drum. A less-dense flowing layer containing a mix of particles gradually develops at the top of the bed, before the percolation mechanism becomes effective and starts segregating the particles in the flowing layer according to their radii. This sequence of events is reflected by the transient peaks in the mixing parameter curves. In the rolling and cascading regimes the initial mixing process proceeds more vigorously at higher rotational speeds, while the lower density of the flowing layer makes the percolation process less discriminative to particle size, thus causing the higher transient peak of the mixing parameter. At all velocities beyond the rolling regime, the decay from the peak maximum to the steady state plateau increases with the drum velocity. Swapping the large and small particles in the block-wise segregated starting configuration or, equivalently, rotating the drum in the opposite direction, does not change the outlined mechanism.

For angular drum velocities in the cateracting regime and beyond, an additional effect starts contributing to the initial mixing of the particles. Because of the limited traction between the drum wall and the granular bed, it takes some time before the particles in the dense bottom of the bed have adjusted to the instantaneously introduced angular velocity of the drum, i.e. till $\mathbf{v}_i \approx \boldsymbol{\omega}_\mathrm{d} \times \mathbf{r}_i$. This transient regime characterized by pronounced slippage at the wall, which will be more pronounced and longer lived at higher angular drum velocities, appears to contribute to the mixing of the particles. Consequently, it might be possible to improve the degree of mixing by prolonging this slip regime. To validate these statements, we simulate two drums whose rotational velocities of 6.28 rad/s and 15 rad/s respectively are alternated after every w revolutions, with w ranging from 1.5 to 6. For a drum velocity of one revolution per second, the effects of periodic rotation reversals are rather limited, see Figure 11. Noticeable deviations from the clock-wise rotating reference system are only observed under frequent reversals, for $w = 1.5$ and 2.5, which are found to slow down the mixing behavior. Yet, after a dozen revolutions (ignoring the rotation direction) all alternating systems have converged to the same steady state as the reference system. The effects of alternating rotation directions are more pronounced at the higher drum velocity of 15 rad/s, see Figure 12, where the steady state degree of mixing steadily increases with the alternation frequency. Note that the mixing parameter still passes through a maximum, after 5 to 10 revolutions, before a gradual decrease sets in. Extending these simulations to nearly 70 revolutions confirms that the steady states have been reached after 30 revolutions, and hence that the higher degree of mixing at lower w is not caused by a slowing down of the segregation. These simulations therefore confirm the above suggestion that mixing maybe promoted by exploiting slippage at the wall.

Fill level

Besides the angular velocity of the drum, the fill level of the drum offers a second easily controlled experimental parameter in the mixing or segregation of granular matter. Figure 13 presents the evolutions of mixing parameters in simulations with fill levels ranging from 25% to 80%, in a drum rotating at 1.57 rad/s. The initial parts of these curves are

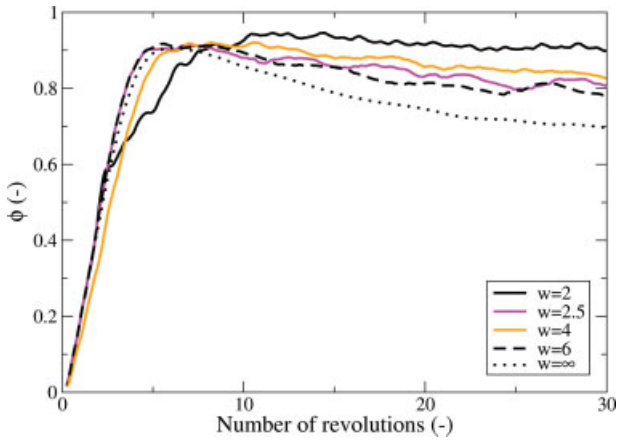

Figure 12. Reversing the rotational direction of the drum every *w* revolutions, in half-filled drums rotating at ±15 rad/s, intensifies the steady state degree of mixing.

The simulations lasted for a total of 40 revolutions, but all significant changes in the order parameters occurred inside the depicted range of revolutions. [Color figure can be viewed in the online issue, which is available at www.interscience.wiley.com.]

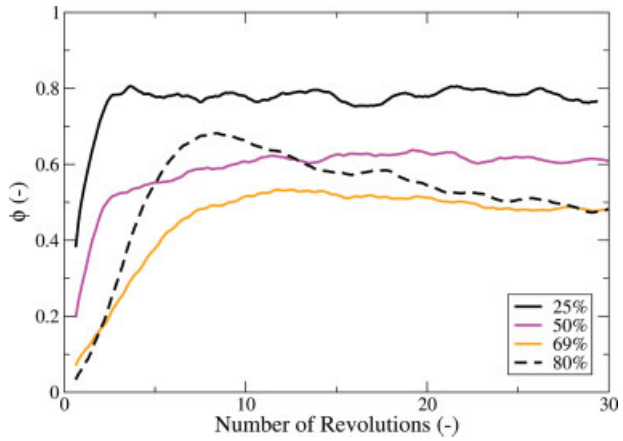

Figure 13. Development of the mixing parameter in drums of various fill levels, all rotating at 1.57 rad/s.

The simulations lasted for a total of 40 revolutions, but all significant changes in the order parameters occurred inside the depicted range of revolutions. [Color figure can be viewed in the online issue, which is available at www.interscience.wiley.com.]

similar to the results presented by Dury and Ristow,[7] who simulated only the first 5–8 revolutions. At the low fill fraction of 25% the particle bed is forced to turn over quicker than the drum, resulting in vigorous motions that keep the bed in a mixed state.[2] Higher fill fractions of about 50% see a less active bed, a decrease in the mixing velocity and a lower final mixing parameter. These two curves are approximated reasonably well by an exponential saturating function, $\phi(t) = \phi_\infty(1 - e^{-t/t_c})$, with t_c the characteristic relaxation time and ϕ_∞ the steady state mixing parameter.[7] As discussed before: while the blockwise segregated bed is being mixed during the first couple of drum revolutions, a gradual build-up of a mixed flowing layer activates the percolation mechanism which in turn results in the exponential approach of the steady state.

The above sequence of events changes at the highest fill fractions ($\geq$69%). Since the initial mixing process is most effective near the top layer of the bed, which now constitutes a relatively small fraction of the total bed, it is becoming difficult to mix the entire bed. After several revolutions the outside region of the bed is reasonably mixed, while the centre of the drum is still in its pristine condition. This unmixed core continues to perform solid body rotations, while the outside region is gradually segregating. Once in a while a large particle drifts away from the core and slowly moves towards the drum wall over many revolutions. Consequently, the unmixed core gradually disappears due to the small residual frictional forces within the bulk of the bed. The mixing curves at these high fill levels show a pronounced local maximum after about 8 revolutions, see the curve for 80% fill level in Figure 13, coinciding with the mixed outside region, followed by a slow decrease due to segregation of the outside region and the even slower disappearance of the unmixed core. These curves can therefore not be fitted adequately by a single exponential relaxation function. Although it is not clear whether a steady state has been reached after the simulated 30 revolutions, the plot strongly suggests that the final degree of mixing ϕ_∞ at 80% fill level will be at least as low as for a 69% fill level. This conclusion is at variance with the prediction by Dury and Ristow[7] that the optimum degree of segregation is obtained at a fill level of about 65%, which was based on extrapolations of their short simulations using the above saturation function.

Rotational speed and fill level

As discussed in the preceding two subsections, both the velocity of rotation and the fill level of the drum affect the dynamics and the mixing or segregation of the granular bed. To investigate their combined impacts on these processes, we have performed ~50 simulations with angular velocities

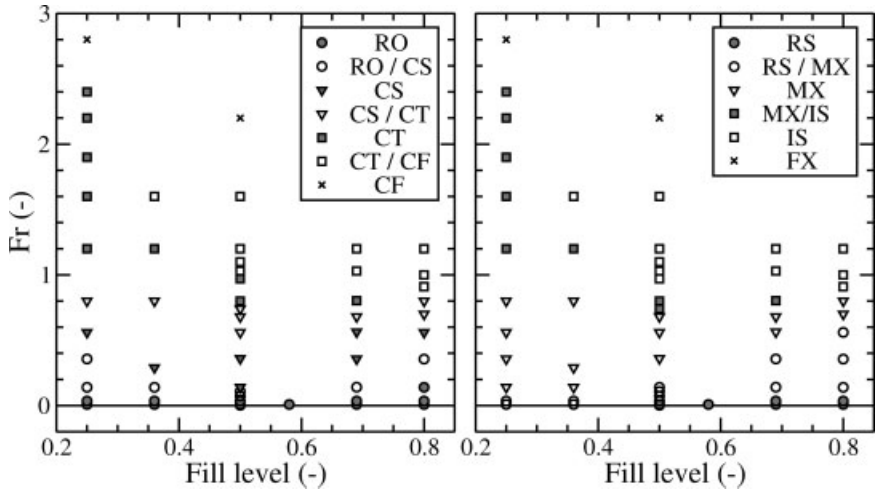

Figure 14. Bed behavior diagrams of the flow regime (left) and the segregation state (right) plotted against the fill fraction and the Froude number.

The markers are used to indicate different stationary states, see the legends to the plots.

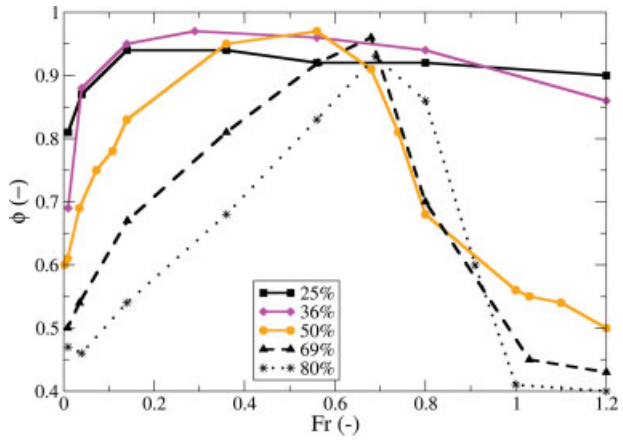

Figure 15. The mixing parameter of the steady state as a function of the Froude number, for various fill factors.

[Color figure can be viewed in the online issue, which is available at www.interscience.wiley.com.]

ranging from 1.57 to 28 rad/s and fill fractions between 25% and 92%. Each run typically lasted for 35–50 revolutions, allowing the systems sufficient time to reach their steady states. The results of these simulations are collected in Figure 14. The left bed behavior diagram in Figure 14 shows the flow regime as a function of the Froude number and the fill factor. Mellmann[19] extensively discusses the bed behavior diagrams of monodisperse systems, comparing theoretical models with experimental findings on near-monodisperse gravel, limestone and sand for fill levels up to 50%. The experimental bed behavior diagrams are qualitatively very similar, and also show a remarkable resemblance to our simulation results on bidisperse systems. It appears, therefore, that the global structure of the bed behavior diagram is rather insensitive to the size distribution of the particles in the granular bed. The right panel of Figure 14 depicts the bed behavior diagram of the segregation in the steady state, again as a function of the Froude number and the fill factor. Comparing this segregation diagram with the flow behavior diagram in the left panel, we note a strong overall resemblance, providing additional support for the correlation between flow regime and segregation pattern. The most pronounced differences are found for low Froude numbers in combination with low fill factors, where the high turn-over rate of the bed relative to the drum causes mixing of the bed.

Figure 15 shows the mixing parameter as a function of the Froude number for a series of fill levels. At any given fill level, the degree of mixing at first improves with increasing velocity of rotation, passes through a maximum, and then decreases again. The Froude number yielding the maximum degree of mixing gradually rises from about 0.1 at 25% filling to 0.7 for a 80% filled drum, while the width of the region with near-maximum mixing strongly decreases with the fill level. The granular bed displays radial segregation for Froude numbers below the broad maximum, while Froude numbers at the opposite side of the maximum create inverted segregated beds (not visible from the plot).

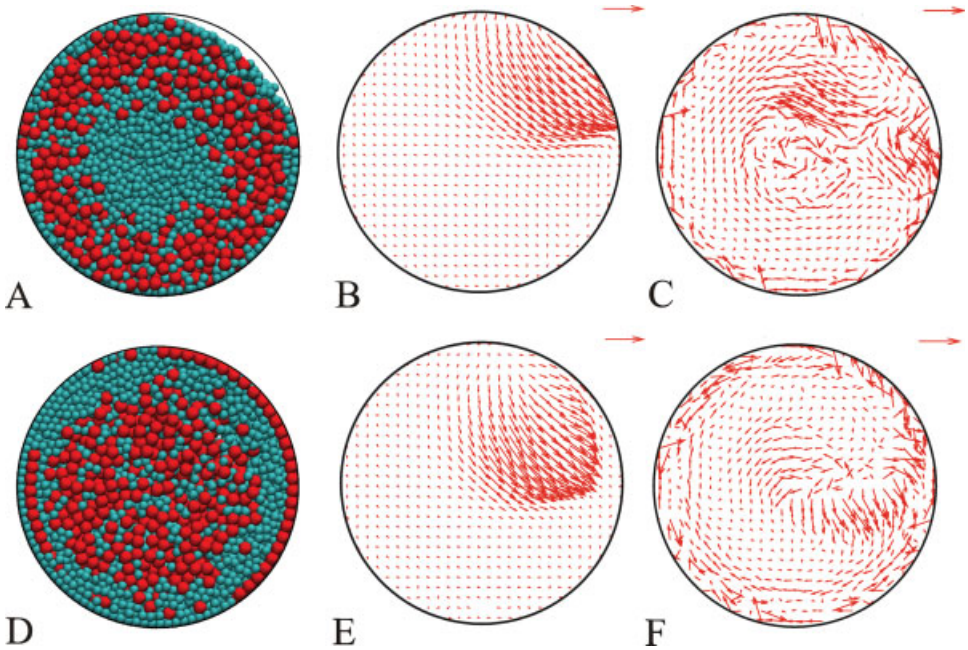

Figure 16. Analysis of the bed properties in rotating 92% filled drums in the cataracting regime (16 rad/s; plots A, B and C) and the cataracting-centrifuging regime (18 rad/s; plots D, E, and F), showing snapshots after 100 revolutions (A and D), relative velocities (B and E with the reference arrows measuring 0.3 m/s) and velocity differences (C and F with the reference arrows indicating 0.05 m/s).

See the caption of Figure 4 for more details. [Color figure can be viewed in the online issue, which is available at www.interscience.wiley.com.]

The highest fill level in our simulations is 92%, but these results have been excluded from the bed behavior diagrams in Figure 14 for clarity. On the one hand, the segregation process proceeds very slowly at these high fill levels, because there is hardly any space available to shuffle the particles. Even after 100 revolutions we are not sure whether the beds have reached their steady states. On the other hand, these runs reveal a number of new segregation forms, making the bed behavior diagram even more complex. For Froude numbers between 0.8 and 1.1 the bed displays double segregation: an inner core of small particles and an outer ring of small particles are separated by a ring of large particles, see Figure 16A. The ring of large particles starts to contain small particles at $Fr = 1$. Figure 16D shows how the ring and core have merged at $Fr = 1.3$ (19 rad/s) to form a large mixed region. One may speculate that this system evolves very slowly and hence that a continuation of the run beyond the current 100 revolutions might show a further development into an inversely segregated state. The velocity plots in Figure 16 show that the beds are again performing solid body rotations, except for the flowing layer in the top right region of the drum. The velocity difference plots are surprisingly rich, with segregation taking place everywhere along the drum wall, in the center of the drum and in the flowing region. Since the formation of a double segregated system might be particularly sensitive to the drum depth, a drum of twice the original length was used to repeat the simulations at 15 and 16.5 rad/s, but these taller drums revealed no significant differences.

Conclusions

The mixing and segregation of bidisperse granules in a rotating short cylindrical drum have been simulated using the Discrete Element Method (DEM). The influence of two easily tunable operational parameters of the drum, namely the fill level and the velocity of revolution were investigated. By varying these two parameters, a number of distinct radial segregation patterns are observed in the bed, as well as near homogeneous mixing of the granules. The flow of the granules in the bed also strongly varies with the operational parameters of the drum. Bed behavior diagrams of the segregation pattern and the flow regime, plotted against the fill level and the drum velocity, are presented in Figure 14. The strong correlation between the two diagrams is indicative of their common origin. A detailed analysis of the granular motions in the various flow regimes, as described in the 'Results and Discussion' section, suggests that the segregation is causally linked to the flow regime by a percolation mechanism: the smaller particles are more likely to fall through the voids in the flowing layer than the larger particles. This selective process, repeated over a number of drum revolutions, gives rise to the separation of small and large particles. The flow regime of the granular bed determines the location, size and density of the flowing layer, and thereby also determines the emerging segregation pattern and its rate of formation.

An interesting observation is that the simulation of a half-filled drum displays inverse segregation at a Froude number of $\sim$0.8. The granules are not yet centrifuging in this simulation, since this Froude number lies well below unity. This observation is therefore not reconcilable with the previous explanation of inverse segregation as resulting from a small difference in the critical centrifuging velocities of small and large particles. Note that the minimum Froude number for inverse segregation will depend on the fill level and various other properties of the granules and the drum, and may therefore approach unity in certain systems.

The sieving action of the percolation mechanism can only be active if both small and large particles are present in the flowing layer. A block-wise segregated starting configuration therefore requires several revolutions, during which the particles are being mixed, before the percolation mechanism effectively starts to segregate the particles. Visualization of the simulations clearly shows that block-wise segregated systems mix before they segregate radially. This behavior is also apparent from the time evolution of the degree of mixing, which in many systems rapidly rises to a local maximum after 5–10 revolutions before gradually decaying to the steady state value. At fill levels beyond 65% only the outer region of the bed is mixed during the initial revolutions, and an unmixed core remains. These systems segregate very slowly, and only gradually lose their unmixed core. By running long simulations it is observed that these systems eventually segregate better than half-filled drums, in contrast to previous reports. At the highest fill level studied (92%) we observe double segregation at $0.8 < \mathrm{Fr} < 1.1$, but because of the extremely slow evolution of this system it can not be ruled out that this pattern is of a transient nature.

Acknowledgments

This project was financially supported through a grant from the Program Economy, Ecology and Technology (E.E.T.) by The Netherlands' Department of Economic Affairs, the Department of Public Housing, Spatial Planning and Environmental Protection, and the Department of Education, Cultural Affairs and Sciences. The authors thank M.A. Boon (TNO Quality of Life, Zeist, The Netherlands) and J.C. Akkerman (TNO Quality of Life, Zeist, The Netherlands) for fruitful discussions.

Literature Cited

1. Jain N, Ottino JM, Lueptow RM. Regimes of segregation and mixing in combined size and density granular systems: an experimental study. *Granular Matter*. 2005;7:69–81.
2. Ottino JM, Khakhar DV. Mixing and segregation of granular materials. *Annu Rev Fluid Mech*. 2000;32:55–91.
3. Rapaport DC. Radial and axial segregation of granular matter in a rotating cylinder: a simulation study. *Phys Rev E*. 2007;75: 031301.1–031301.11.
4. Cleary PW, Metcalfe G, Liffman K. How well do discrete element granular flow models capture the essentials of mixing processes? *Appl Math Model*. 1998;22:995–1008.
5. Boateng AA, Barr BV. Modelling of particle mixing and segregation in the transverse plane of a rotary kiln. *Chem Eng Sci*. 1996;51: 4167–4181.
6. Dury CM, Ristow GH. Radial segregation in a two-dimensional rotating drum. *J de Phys I*. 1997;7:737–745.
7. Dury CM, Ristow GH. Competition of mixing and segregation in rotating cylinders. *Phys Fluids*. 1999;11:1387–1394.
8. Nityanand N, Manley B, Henein H. An analysis of radial segregation for different sized spherical solids in rotary cylinders. *Metall Trans B Process Metall*. 1986;17:247–257.
9. Turner JL, Nakagawa M. Particle mixing in a nearly filled horizontal cylinder through phase inversion. *Powder Technol*. 2000;113:119–123.
10. Donald M, Roseman B. Mixing and Demixing of Solid Particles. Part 1. Mechanisms in a horizontal drum mixer. *Br Chem Eng*. 1962;7:749–752.

11. Hill KM, Caprihan A, Kakalios J. Bulk segregation in rotated granular material measured by magnetic resonance imaging. *Phys Rev Lett*. 1997;78:50–53.
12. Rapaport DC. Simulational studies of axial granular segregation in a rotating cylinder. *Phys Rev E*. 2002;65:061306.1–061306.11.
13. Hill KM, Gioia G, Amaravadi D. Radial segregation patterns in rotating granular mixtures: Waviness selection. *Phys Rev Lett*. 2004;93: 224301.1–224301.4.
14. Khakhar DV, Orpe AV, Hajra SK. Segregation of granular materials in rotating cylinders. *Phys Stat Mech Appl*. 2003;318:129–136.
15. Khakhar DV, Orpe AV, Ottino JM. Continuum model of mixing and size segregation in a rotating cylinder: concentration-flow coupling and streak formation. *Powder Technol*. 2001;116:232–245.
16. Hajra SK, Khakhar DV. Sensitivity of granular segregation of mixtures in quasi-two-dimensional fluidized layers. *Phys Rev E*. 2004; 69(3 Part 1):031304.
17. Eskin D, Kalman H. A numerical parametric study of size segregation in a rotating drum. *Chem Eng Process*. 2000;39:539–545.
18. Henein H, Brimacombe JK, Watkinson AP. Experimental-study of transverse bed motion in rotary kilns. *Metall Trans B Process Metall*. 1983;14:191–205.
19. Mellmann J. The transverse motion of solids in rotating cylinders—forms of motion and transition behavior. *Powder Technol*. 2001; 118:251–270.
20. Chakraborty S, Nott PR, Prakash JR. Analysis of radial segregation of granular mixtures in a rotating drum. *Eur Phys J E*. 2000;1:265–273.
21. Ding YL, Forster R, Seville JPK, Parker DJ. Segregation of granular flow in the transverse plane of a rolling mode rotating drum. *Int J Multiphase Flow*. 2002;28:635–663.
22. Felix G, Thomas N. Evidence of two effects in the size segregation process in dry granular media. *Phys Rev E*. 2004;70(5 Part 1):051307.
23. Khakhar DV, McCarthy JJ, Ottino JM. Radial segregation of granular mixtures in rotating cylinders. *Phys Fluids*. 1997;9:3600–3614.
24. Santomaso AC, Ding YL, Lickiss JR, York DW. Investigation of the granular behavior in a rotating drum operated over a wide range of rotational speed. *Chem Eng Res Des*. 2003;81:936–945.
25. Zuriguel I, Gray J, Peixinho J, Mullin T. Pattern selection by a granular wave in a rotating drum. *Phys Rev E*. 2006;73(6 Part 1): 061302.
26. Finnie GJ, Kruyt NP, Ye M, Zeilstra C, Kuipers JAM. Longitudinal and transverse mixing in rotary kilns: A discrete element method approach. *Chem Eng Sci*. 2005;60:4083–4091.
27. Lai FS, Fan LT. Application of a discrete mixing model to study of mixing of multicomponent solid particles. *Ind Eng Chem Process Des Dev*. 1975;14:403–411.
28. Masiuk S, Rakoczy R. The entropy criterion for the homogenisation process in a multi-ribbon blender. *Chem Eng Process*. 2006;45:500–506.
29. Schutyser MAI, Weber FJ, Briels WJ, Boom RM, Rinzema A. Three-dimensional simulation of grain mixing in three different rotating drum designs for solid-state fermentation. *Biotechnol Bioeng*. 2002;79:284–294.
30. Savage SB, Lun CKK. Particle-size segregation in inclined chute flow of dry cohesionless granular solids. *J Fluid Mech*. 1988; 189: 311–335.
31. Cundall PA, Strack ODL. Discrete numerical-model for granular assemblies. *Geotechnique*. 1979;29:47–65.
32. Hoomans BPB. Granular dynamics of gas-solid two-phase flows. PhD thesis. Enschede, The Netherlands, University of Twente, 2000.
33. Poschel T, Herrmann HJ. Size segregation and convection. *Europhys Lett*. 1995;29:123–128.
34. Thompson PA, Grest GS. Granular flow—friction and the dilatancy transition. *Phys Rev Lett*. 1991;67:1751–1754.
35. Schafer J, Dippel S, Wolf DE. Force schemes in simulations of granular materials. *J de Phys I*. 1996;6:5–20.
36. Allen MP, Tildesley DJ. *Computer Simulation of Liquids*. Oxford, UK: Oxford Science Publications, 1987.
37. Schutyser MAI, Padding JT, Weber FJ, Briels WJ, Rinzema A, Boom R. Discrete particle simulations predicting mixing behavior of solid substrate particles in a rotating drum fermenter. *Biotechnol Bioeng*. 2001;75:666–675.
38. Porion P, Sommier N, Faugere AM, Evesque P. Dynamics of size segregation and mixing of granular materials in a 3D-blender by NMR imaging investigation. *Powder Technol*. 2004;141:55–68.
39. Van Puyvelde DR. Simulating the mixing and segregation of solids in the transverse section of a rotating kiln. *Powder Technol*. 2006; 164:1–12.
40. Metcalfe G, Shinbrot T, McCarthy JJ, Ottino JM. Avalanche mixing of granular solids. *Nature*. 1995;374:39–41.
41. Humphrey W, Dalke A, Schulten K. VMD: Visual molecular dynamics. *J Mol Graph*. 1996;14:33–38, 27–28.
42. Walton OR, Braun RL. Stress calculations for assemblies of inelastic spheres in uniform shear. *Acta Mechanica*. 1986;63:73–86.
43. McCarthy JJ, Ottino JM. Particle dynamics simulation: a hybrid technique applied to granular mixing. *Powder Technol*. 1998;97:91–99.
44. Tsuji Y, Tanaka T, Ishida T. Lagrangian numerical-simulation of plug flow of cohesionless particles in a horizontal pipe. *Powder Technol*. 1992;71:239–250.
45. Nakagawa M, Altobelli SA, Caprihan A, Fukushima E, Jeong EK. Noninvasive measurements of granular flows by magnetic-resonance-imaging. *Exp Fluids*. 1993;16:54–60.
46. Eskin D, Kalman H. Optimal particle acceleration in a centrifugal rotor-impact mill. *Miner Eng*. 2000;13:1653–1658.

Manuscript received Apr. 3, 2008, and revision received Jun. 12, 2008.